




Article

High Active and Selective Ni/CeO₂–Al₂O₃ and Pd–Ni/CeO₂–Al₂O₃ Catalysts for Oxy-Steam Reforming of Methanol

Paweł Mierczynski ^{1,*} , Agnieszka Mierczynska ² , Radosław Ciesielski ¹,
Magdalena Mosinska ¹, Magdalena Nowosielska ¹, Agnieszka Czyłkowska ¹,
Waldemar Maniukiewicz ¹ , Małgorzata I. Szyńska ¹ and Krasimir Vasilev ³

¹ Institute of General and Ecological Chemistry, Lodz University of Technology, Zeromskiego 116, 90-924 Lodz, Poland; radoslaw.ciesielski@p.lodz.pl (R.C.); m.mosinska@op.pl (M.M.); magdalena.nowosielska@p.lodz.pl (M.N.); agnieszka.czyłkowska@p.lodz.pl (A.C.); waldemar.maniukiewicz@p.lodz.pl (W.M.); malgorzata.szynkowska@p.lodz.pl (M.I.S.)

² The Australian Wine Research Institute, Waite Precinct, Hartley Grove cnr Paratoo Road, Adelaide 5064, Australia; agnieszka.mierczynska-vasilev@awri.com.au

³ School of Engineering, University of South Australia, Mawson Lakes 5095, Australia; krasimir.vasilev@unisa.edu.au

* Correspondence: pawel.mierczynski@p.lodz.pl; Tel.: +48-42-631-31-24; Fax: +48-42-631-31-28

Received: 2 August 2018; Accepted: 2 September 2018; Published: 6 September 2018



Abstract: Herein, we report monometallic Ni and bimetallic Pd–Ni catalysts supported on CeO₂–Al₂O₃ binary oxide which are highly active and selective in oxy-steam reforming of methanol (OSRM). Monometallic and bimetallic supported catalysts were prepared by an impregnation method. The physicochemical properties of the catalytic systems were investigated using a range of methods such as: Brunauer–Emmett–Teller (BET), X-ray Powder Diffraction (XRD), Temperature-programmed reduction (TPR–H₂), Temperature-programmed desorption (TPD–NH₃), X-ray photoelectron spectroscopy (XPS) and Scanning Electron Microscope equipped with an energy dispersive spectrometer (SEM–EDS). We demonstrate that the addition of palladium facilitates the reduction of nickel catalysts. The activity tests performed for all catalysts confirmed the promotion effect of palladium on the catalytic activity of nickel catalyst and their selectivity towards hydrogen production. Both nickel and bimetallic palladium–nickel supported catalysts showed excellent stability during the reaction. The reported catalytic systems are valuable to make advances in the field of fuel cell technology.

Keywords: OSRM; nickel; bimetallic catalyst; heterogeneous catalysis; Pd–Ni

1. Introduction

Over the last decades there have been substantial efforts to develop environmentally friendly sources of energy capable of replacing fossil fuels [1–3]. One of the sources that has captured attention is hydrogen since it combusts without the release of pollutants [4–10]. The increased interest in hydrogen is associated with the use of hydrogen to power fuel cells [11,12] as one alternative to replace currently dominant fossil fuels.

Hydrogen can be produced by decomposition of methanol and via steam or oxygen reforming of methanol. These reactions can be coupled in a single process called oxy-steam reforming of methanol [1,6,13–16]. This is very advantageous from the economic point of view because the process proceeds in an auto-thermal way without the need of external heat. Catalysts are essential to carry

out the processes with high yield and selectivity. Common catalysts used during these processes are copper and nickel based systems supported on mono- and binary oxides [5,14,17–24].

Typically, in methanol reforming reactions, both mono- and binary oxide supports [8,10,13,19,21,25–30] are used. To improve the catalytic activity, stability, and selectivity, different modifiers are added to the catalytic systems. The type of support and its nature as well as the preparation method has a great influence on the Ni based catalyst activity and stability.

The use of CeO₂ as modifiers in Ni based catalysts has been reported. It was found that the introduction of cerium (IV) oxide into nickel based catalysts improves the metallic dispersion, limits particles agglomeration, and enhances the metal-support interaction. All of these factors have a positive effect on the catalytic activity of nickel supported catalysts in dry reforming of methane [31]. Li et al. [32] studied CeO₂-promoted Ni/Al₂O₃-ZrO₂ catalyst in methane reforming with CO₂. They found that addition of CeO₂ into monometallic nickel effectively improves the dispersion of Ni particles on the catalyst surface and enhances the stability of the nickel catalyst. The authors also reported an increased CO₂ adsorption on the catalyst surface after the introduction of CeO₂. Ahmed et al. [33] investigated the effect of ceria on the catalytic activity of Ni/CeO₂-Al₂O₃ systems in thermo-catalytic decomposition of methane. The results confirmed that ceria itself has great influence on the catalytic activity and stability. It was also demonstrated that CeO₂ influences the size of Ni particle and the catalyst morphology. The reducibility results confirmed that promotion of Ni/Al₂O₃ catalyst by CeO₂ inhibits nickel aluminate formation. The promotion of copper catalyst by CeO₂ also leads to an increase the thermal stability [34]. In addition, cerium (IV) oxide can provide mobile oxygen which has a direct influence on the catalytic activity and may affect the valance state of the metal present on the support surface under a reducing environment.

An attractive route for CeO₂-Al₂O₃ synthesis is the co-precipitation method [35]. The binary oxide prepared by this method allows better dispersion of the active species to be obtained on its surface compared to catalysts supported on bi-oxide carrier prepared by impregnation methods [36]. The activity results performed over Ni catalysts supported on monoxide CeO₂ and Al₂O₃ and binary CeO₂-Al₂O₃ oxide in methane thermo-catalytic decomposition shows that Ni/CeO₂-Al₂O₃ systems have better catalytic properties compared to the mono-oxides [33]. It was also proven that the CeO₂ content [33] and the treatment conditions of the synthesized CeO₂-Al₂O₃ carrier have great influence on their catalytic and physicochemical properties. It is also well documented that the preparation method of the support has a large impact on its physical and chemical properties [37,38]. The selection of a suitable preparation method of binary oxide is important to ensure appropriate interaction between the support and the active phase component.

It is also well documented that promotion of monometallic catalysts by precious metals in most cases improves the catalyst activity [13], stability, and selectivity in the methanol reforming processes. The addition of precious metals to monometallic catalysts facilitates their reduction and affects their acidic and electron properties. Palladium is an active component for methanol reforming reactions. It is an effective decomposition catalyst, selectively forming H₂ and CO when it is supported on metal oxide [39–41]. However, when palladium is supported on ZnO, high selectivity for CO₂ in the steam reforming of methanol (SRM) reaction has been reported. This change in selectivity can be explained by the Pd-Zn alloys formation [42]. These palladium alloys are formed at moderate temperatures under reducing conditions [43].

2. Results and Discussion

2.1. Catalytic Performance in Oxy-Steam Reforming of Methanol

The catalytic activity tests in oxy-steam reforming of methanol were performed at two temperatures, 200 and 250 °C, respectively. The results of the activity are expressed as methanol conversion and selectivity towards all products and are given in Table 1. The activity results showed that conversion of methanol increases with increase of the metal content. The highest methanol

conversion among all tested nickel catalysts was shown by the 40%Ni/CeO₂–Al₂O₃ system which also had the highest hydrogen yield at 250 °C. A further increase in the nickel content caused a decrease in catalytic activity. The reactivity results confirmed the promotion effect of palladium when added to nickel catalyst on methanol conversion at both reaction temperatures. In addition, palladium enhanced the selectivity of the nickel catalyst towards hydrogen formation (see Table 1). To better understand the influence of the support composition on the catalytic activity in oxy-steam reforming of methanol (OSRM) analogous tests were performed on nickel catalysts supported on Al₂O₃ or CeO₂ monoxides containing the same nickel content. The activity results are given in the same Table 1. The results indicate higher activity of 40%Ni/CeO₂ compared to 40%Ni/Al₂O₃ but lower than the analogous catalyst supported on binary oxide. It should be noted that Ni catalyst supported on CeO₂ exhibited higher methanol conversion (85%) and high selectivity to hydrogen at 250 °C compared to the Ni/Al₂O₃ system. In comparison, the Ni/Al₂O₃ catalyst showed low methanol conversion (20.5%) at 250 °C and formation of carbon monoxide was not observed during the reaction.

Pérez-Hernández et al. [22] investigated the catalytic properties of monometallic nickel, copper and bimetallic Cu–Ni catalysts supported on ZrO₂ in oxy-steam reforming of methanol. They tested nickel catalyst with low Ni loading (2.44% wt. of Ni) in the OSRM process in the temperature range 250–300 °C (Gas Hourly Space Velocity (GHSV) = 30,000 h^{−1}) and obtained the lowest methanol conversion value below 14% and the lowest selectivity towards hydrogen production, while all investigated catalysts showed comparable selectivity towards H₂ at the maximum reaction temperature (about 60%). However, nickel supported catalysts showed high CO selectivity. The total methanol conversion was obtained for the Ni/ZrO₂ catalyst at a temperature of 350 °C. These findings agree well with our activity results. We also detected only 2% of methanol conversion at 250 °C for the 5%Ni/CeO₂–Al₂O₃ system. Similar reactivity results are shown in other studies [14]. The authors tested monometallic 3% Cu/ZrO₂, 3% Ni/ZrO₂, and bimetallic Ni–Cu systems in OSRM (GHSV = 24,000 h^{−1}) in the temperature range 200–350 °C and confirmed the lowest activity of Ni catalyst in the studied temperature range. At 350 °C nickel catalyst showed below 70% of methanol conversion. The selectivity towards CO production at 350 °C was about 10% for the monometallic Ni and Cu catalysts and about 40% for the bimetallic supported catalysts. The results of the selectivity towards hydrogen production showed that bimetallic catalysts exhibited high hydrogen yield close to the theoretical value. However, monometallic systems showed about 60% of the hydrogen yield in the OSRM reaction.

In the next step of our reactivity studies we tested the stability of both monometallic nickel and bimetallic Pd–Ni catalysts in oxy-steam reforming of methanol. The results of the stability tests in OSRM on monometallic nickel and bimetallic Pd–Ni catalysts supported on CeO₂–Al₂O₃ within 48 h are presented in Figure 1. Both mono- and bimetallic catalysts exhibited high and stable activity and selectivity towards hydrogen production at the investigated temperature. López et al. [14] investigated the stability of the bimetallic Cu–Ni/ZrO₂ catalysts in the oxy-steam reforming process within 50 h at a temperature of 300 °C. They also monitored the methanol conversion and selectivity towards hydrogen production values. The stability tests performed within 50 h on stream showed high stability of the catalyst. The methanol conversion was stable and equal to about 85%. However, the selectivity towards hydrogen was low and only reached values around 43%. Our catalytic systems showed markedly higher activity and selectivity towards hydrogen production. The stability tests showed that both monometallic and bimetallic catalysts exhibited high activity reaching 100% and the selectivity towards hydrogen formation was in the range of 70%. These activity and stability tests confirmed that the prepared catalysts could be potentially applied in fuel cell technology to produce the hydrogen needed to power them.

Table 1. Effect of temperature on the catalytic activity and selectivity to hydrogen, carbon monoxide, carbon dioxide, dimethyl ether (DME) in oxy-steam reforming of methanol over monometallic Ni catalysts supported on Al_2O_3 , CeO_2 , $\text{CeO}_2\text{-Al}_2\text{O}_3$ and bimetallic Pd–Ni catalysts supported on binary oxide $\text{CeO}_2\text{-Al}_2\text{O}_3$. Reaction condition: weight of catalyst = 0.2 g, $\text{H}_2\text{O}/\text{CH}_3\text{OH}/\text{O}_2$ molar ratio in the reaction mixture = 1/1/0.4, temperature of the reaction 200 and 250 °C. The catalytic tests were performed under atmospheric pressure (Gas Hourly Space Velocity (GHSV) = 26,700 h^{-1}).

Catalyst	CH ₃ OH Conv. (%)		H ₂ Selectivity (%)		CO Selectivity (%)		CO ₂ Selectivity (%)		DME Selectivity (%)	
	200 °C	250 °C	200 °C	250 °C	200 °C	250 °C	200 °C	250 °C	200 °C	250 °C
5%Ni/CeO ₂ -Al ₂ O ₃	-	2	-	30.5	-	-	-	25	-	44.5
20%Ni/CeO ₂ -Al ₂ O ₃	11	31	66.5	33	-	-	26.3	55.6	7.2	11.4
40%Ni/CeO ₂ -Al ₂ O ₃	40	98	45.2	68.9	46	13.3	8.3	14.3	0.5	3.5
60%Ni/CeO ₂ -Al ₂ O ₃	18	77	61.4	58.2	-	27.7	38.6	14.1	-	trace
40%Ni/CeO ₂	4	85	75	68.6	24.2	22.6	-	0.5	0.8	8.3
40%Ni/Al ₂ O ₃	-	20.5	-	53.4	-	-	-	25.2	-	21.4
2%Pd-40%Ni/CeO ₂ -Al ₂ O ₃	67	99.9	70.3	71.5	21.8	14.9	7.6	9.1	0.3	4.5

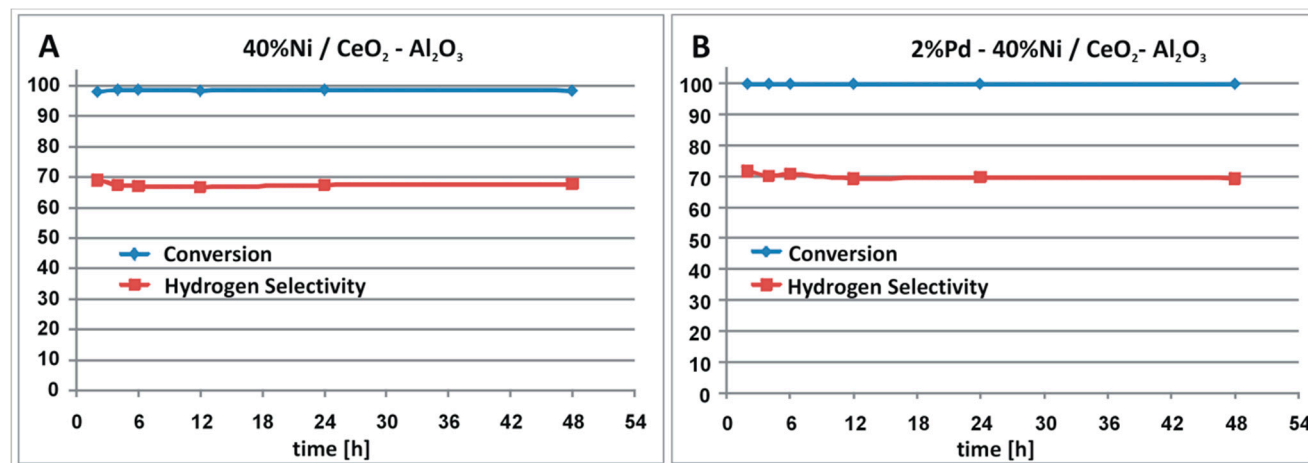


Figure 1. Methanol conversion and selectivity towards hydrogen formation for (A) monometallic Ni/CeO₂-Al₂O₃ supported catalyst; and (B) bimetallic Pd–Ni/CeO₂-Al₂O₃ during 48 h of the reaction performed at 250 °C after reduction 1 h at 300 °C in a mixture of 5% H_2 –95%Ar.). Reaction condition: weight of catalyst = 0.2 g, $\text{H}_2\text{O}/\text{CH}_3\text{OH}/\text{O}_2$ molar ratio in the reaction mixture = 1/1/0.4, temperature of the reaction 200 and 250 °C. The catalytic tests were performed under atmospheric pressure (Gas Hourly Space Velocity (GHSV) = 26,700 h^{-1}).

2.2. Specific Surface Area and Chemisorption Measurements

Specific surface area (SSA) measurements were performed for all catalytic systems and the results are given in Table 2. The SSA results showed that the highest specific surface area had aluminium oxide. On the other hand, cerium (IV) oxide was characterized by the lowest specific surface area of $60 \text{ m}^2/\text{g}$. The $\text{CeO}_2\text{-Al}_2\text{O}_3$ system had an intermediate value of specific surface area. The addition of nickel oxide into the catalytic support caused the decrease of the specific surface area of the support. This is due to the blockage of the support pores by metal oxide phase which is an active component of the catalyst. An analogous behaviour was observed for the nickel supported catalytic systems after palladium addition, the same trend was observed for the monolayer capacity results. The addition of the active phase component results in a decrease of the monolayer capacity values independently of the catalyst support used. The results are in agreement with those published for monometallic nickel supported catalysts [33].

Chemisorption measurements performed for nickel catalysts showed that the highest nickel dispersion degree had the 20%Ni/ $\text{CeO}_2\text{-Al}_2\text{O}_3$ catalyst while the lowest dispersion degree showed 60%Ni/ $\text{CeO}_2\text{-Al}_2\text{O}_3$ catalyst. It should be also mentioned that the 20%Ni/ $\text{CeO}_2\text{-Al}_2\text{O}_3$ catalyst had the highest metallic nickel surface area and exhibited the highest amount of hydrogen adsorbed on the metallic nickel atoms (see Table 2). Among the catalysts with 40% Ni loading, the 40%Ni/ Al_2O_3 catalyst exhibited the highest Ni dispersion degree. However, this system exhibited the lowest methanol conversion at 250°C among all nickel catalysts with the same Ni content. These results suggest that the size of the metallic particles is not a major factor influencing the reactivity properties of the nickel catalyst in OSRM. The evidence of this is the highest methanol conversion of the 40%Ni/ $\text{CeO}_2\text{-Al}_2\text{O}_3$ catalyst at 250°C (see Table 2).

2.3. Reduction Behaviour of Monometallic Ni and Bimetallic Pd–Ni Supported Catalysts

The temperature programmed reduction studies were performed in order to determine the reducibility of the supports (CeO_2 and $\text{CeO}_2\text{-Al}_2\text{O}_3$) and Ni supported catalysts. All TPR- H_2 curves recorded for the investigated samples are given in Figure 2A,B. First, the reduction behaviour of CeO_2 was investigated. The result of the TPR- H_2 study is shown in Figure 2A. The TPR- H_2 curve recorded for CeO_2 oxide system showed two reduction stages. The first hydrogen consumption peak visible in the temperature range of $355\text{--}580^\circ\text{C}$ is connected with the reduction of CeO_2 surface species to non-stoichiometric oxides CeO_{2-x} . The second high-temperature peak located above 670°C is assigned to the bulk CeO_2 reduction [44]. Analogous measurements were carried out for binary oxides. The TPR- H_2 curve showed the same reduction stages observed for monoxide CeO_2 . The reducibility of nickel catalysts supported on monoxide such as Al_2O_3 and CeO_2 or binary oxide system was also studied. The TPR- H_2 profile of Ni/ Al_2O_3 catalyst showed four hydrogen consumption peaks located at about 270 , 420 , 545 , and 750°C , respectively. The observed reduction effects can be associated with the reduction of various nickel (II) oxide species (see Figure 2A). The first peak located at about 270°C is connected with the reduction of free NiO species [45]. The second peak with a maximum reduction rate at 420°C is assigned to the reduction of NiO interacted with support [46]. The third hydrogen consumption peak centred at 545°C is assigned to the reduction of Ni–O–Al linkage species [33,47–49]. The last reduction stage above 650°C is assigned to the reduction of spinel phase NiAl_2O_4 . The reduction behaviour of Ni/ Al_2O_3 was studied previously [33]. The authors also observed four reduction stages in the TPR profile recorded for Ni/ Al_2O_3 catalyst assigned to highly dispersed, free and aggregated NiO species, NiO interacted with support and NiAl_2O_4 species reduction [48].

Table 2. Brunauer–Emmett–Teller (BET) surface area, monolayer capacity and dispersion degree of metallic nickel phase of supports and supported nickel catalysts calcined in air atmosphere for 4 h at 400 °C.

Catalytic Material	BET Surface Area (m ² /g)	Monolayer Capacity (cm ³ /g)	Metal Dispersion (%)	Metal Area (m ² g ^{−1} of Metal)	Crystallite Size (nm)	H ₂ Sorption (μmolH ₂ gcat ^{−1})	X ^a (%)
Al ₂ O ₃	210	48.2	-	-	-	-	-
CeO ₂	60	13.8	-	-	-	-	-
eO ₂ -Al ₂ O ₃	145	33.2	-	-	-	-	-
5%Ni/CeO ₂ -Al ₂ O ₃	132	30.3	1.06	7.09	95.0	0.102	2
20%Ni/CeO ₂ -Al ₂ O ₃	128	29.5	1.16	7.71	87.4	0.442	31
40%Ni/CeO ₂ -Al ₂ O ₃	78	17.9	0.54	3.61	186	0.414	98
40%Ni/Al ₂ O ₃	133	30.5	0.69	4.63	146	0.326	20.5
40%Ni/CeO ₂	34	7.8	0.63	4.18	146	0.479	85
60%Ni/CeO ₂ -Al ₂ O ₃	58	13.2	0.28	1.90	356	0.531	77
2%Pd-40%Ni/CeO ₂ -Al ₂ O ₃	42	9.6	-	-	-	-	99.9

Activation of catalysts: reduction before activity tests in the 5% H₂-95% Ar mixture at 300 °C, 2 h. Reaction conditions: T = 250 °C, m_{cat.} = 0.2 g, CH₃OH/H₂O/O₂ = 1, feed flow rate = 40 mL/min. ^a Methanol conversion at T = 250 °C.

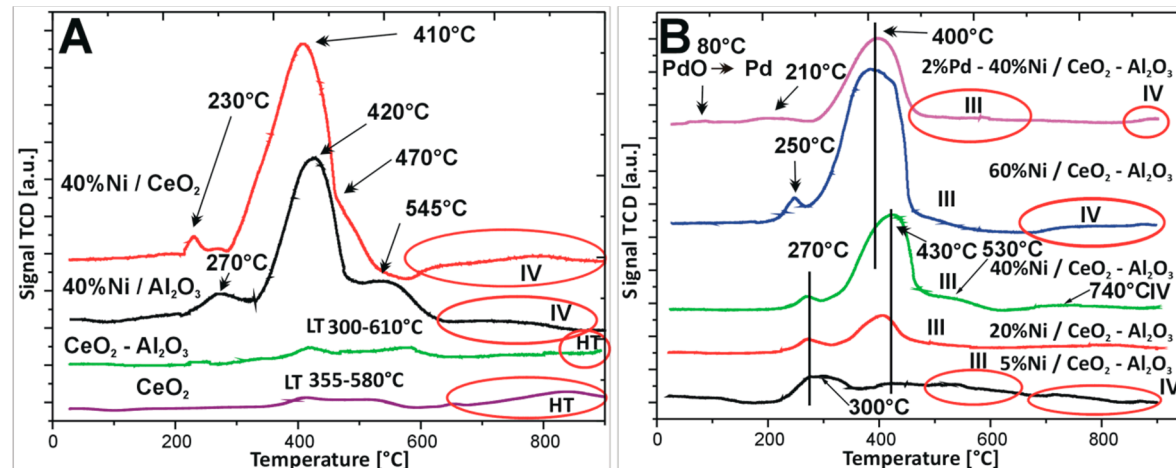


Figure 2. TPR profile of (A) supports CeO₂, CeO₂-Al₂O₃ and monometallic catalysts supported on CeO₂ or Al₂O₃; and (B) monometallic nickel catalysts supported on binary oxide and bimetallic systems after calcination in air atmosphere for 4 h at 400 °C.

The reduction behaviour of Ni/CeO₂ catalyst was also studied in detail. The TPR profile recorded for the system showed a four step reduction (see Figure 2A). The first two effects are assigned to the reduction of free unbound and strongly interacted NiO with support. The same reduction stages were observed for nickel catalyst supported on Ni/Al₂O₃ catalyst [47]. The third stage is assigned to the reduction of surface oxygen species of CeO₂. The last high temperature peak is attributed to the reduction of CeO₂ in bulk [44]. Ahmed et al. [33] also studied the reduction behaviour of Ni catalyst supported on pure CeO₂. They reported about a two-step reduction process of the nickel supported catalyst. The reduction stages located in the temperature range of 300–550 °C were assigned to the reduction of Ce⁴⁺ to non-stoichiometric oxides CeO_{2-x} and also with the reduction of NiO interacted with the support. However, no high temperature effect connected with the reduction of bulk Ce⁴⁺ to Ce³⁺ was reported.

In the next step, the interaction between active phase component and support (CeO₂–Al₂O₃) was investigated for the monometallic nickel and bimetallic Pd–Ni catalysts (see Figure 2B). The TPR profiles of nickel catalysts supported on CeO₂–Al₂O₃ oxide showed four reduction stages in the reduction profiles independently from the nickel content. The TPR profile recorded for 5%Ni/CeO₂–Al₂O₃ catalyst showed the first two reduction stages positioned at 300 and 430 °C which are assigned to the reduction of unbounded NiO species strongly interacted with support. The third reduction peak located in the temperature range of 500–650 °C is attributed to the reduction of surface oxygen species of CeO₂ and Ni–O–Al linkage reduction. The last reduction stage is attributed to the reduction of CeO₂ in bulk as well as to the reduction of spinel NiAl₂O₄ structure. TPR curve of 20%Ni/CeO₂–Al₂O₃ system showed also four stages, which are related to reduction of the same oxides species. The first two reduction peaks are visible at 270 and 430 °C, respectively. The third effect is located in the temperature range of 480–600 °C while the last one is situated above 650 and is completed at 900 °C. Further increase of the Ni content in the catalytic systems did not change the reduction behaviour of the investigated nickel catalysts. The TPR profile of 40%Ni/CeO₂–Al₂O₃ had the same shape as previously described for Ni catalysts. On the other hand, the TPR curve of 60%Ni/CeO₂–Al₂O₃ catalyst exhibited the same reduction stages as for previously presented catalysts the only difference being the location of each effects and their intensity. In the case of the 60%Ni/CeO₂–Al₂O₃ catalyst, the first two effects were visible at 250 and 400 °C and their intensity was significantly higher compared to previously described systems. The third effect was located in the temperature range 450–600 °C. The last high temperature effect (IV) connected with the reduction of CeO₂ in bulk and the reduction of spinel NiAl₂O₄ structure was observed above 680 °C. The reduction process of monometallic Ni catalysts supported on CeO₂–Al₂O₃ systems containing various Ce/Al ratios were investigated previously [33]. The authors reported that their reducible behaviour strongly depends on the catalyst composition. They also observed four stages of reduction of the studied catalysts on the TPR curves as in our case. The reducibility of Ni catalysts supported on CeO₂, Al₂O₃, and CeO₂–Al₂O₃ supports were also reported [50]. The authors also described several reduction peaks in the TPR curves recorded for supported catalysts connected with reduction of three types of NiO species (α , β , and γ). They also claimed that addition of CeO₂ into Al₂O₃ weakens the interaction between the NiO and Al₂O₃.

The last catalytic system which was studied by temperature-programmed-reduction technique was bimetallic Pd–Ni/CeO₂–Al₂O₃ supported catalyst. The TPR–H₂ profile of bimetallic catalyst showed five effects in the reduction profile. The first reduction step positioned at 80 °C is assigned to the reduction of PdO to metallic palladium. The second and third hydrogen consumption peaks located at 210 and 400 °C are assigned to the reduction of unbound and strongly interacted with support NiO species. This means that addition of palladium into nickel supported catalyst facilitates the reduction of NiO species which is confirmed by the shift of the second and third observed reduction profiles towards the lower temperature range compared to the same reduction effects observed in the case of monometallic 40%Ni/CeO₂–Al₂O₃ catalysts. The fourth and fifth hydrogen consumption peaks are positioned at the same temperature as for 40%Ni/CeO₂–Al₂O₃ catalyst. The shift of the

visible second and third effect recorded in the case of bimetallic supported catalysts compared to monometallic catalyst towards low temperature range is due to a spill over phenomenon occurring between metallic palladium and nickel oxide. Hydrogen dissociates on palladium and then atomic hydrogen spills over from metallic palladium to nickel oxide, causing its reduction.

2.4. XRD Structural Analysis

The analysis of the diffraction curves recorded for monometallic nickel supported catalysts calcined in air for 4 h at 400 °C showed the presence of only NiO and CeO₂ phases, independently of the nickel content (see Figure 3). This is supported in published studies [51,52]. Ahmed et al. [33] studied the phase composition of as prepared CeO₂–Al₂O₃ binary oxide and mono-oxides such as: CeO₂ and Al₂O₃ supports calcined in air at 550 °C. They reported the presence of θ -Al₂O₃ phase, γ -Al₂O₃, and crystalline CeO₂ cubic fluorite structure phases for the investigated supports.

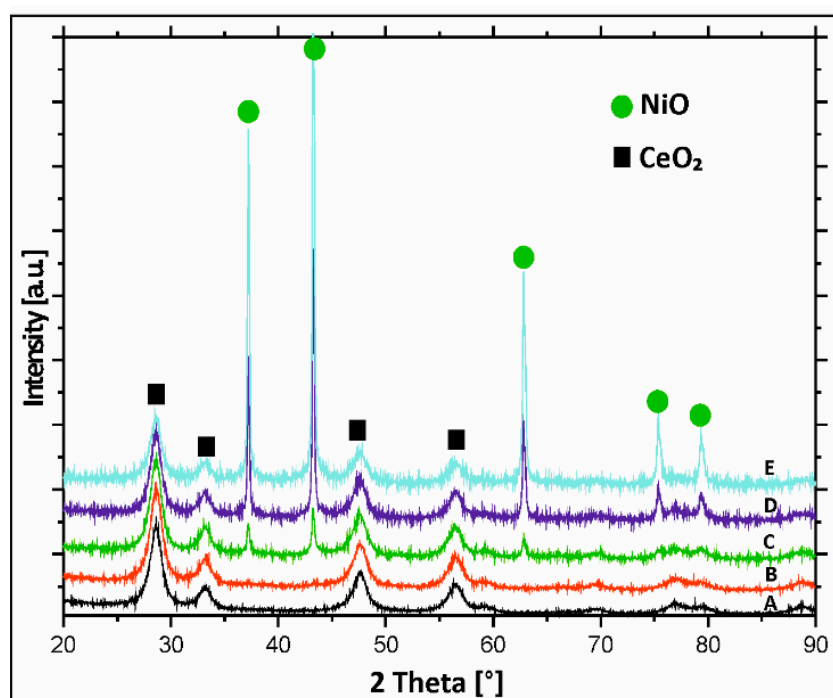


Figure 3. X-ray powder patterns of calcined (A) binary oxide and monometallic; (B) 5%Ni/CeO₂–Al₂O₃; (C) 20%Ni/CeO₂–Al₂O₃; (D) 40%Ni/CeO₂–Al₂O₃; and (E) 60%Ni/CeO₂–Al₂O₃ catalysts in an air atmosphere for 4 h at a temperature of 400 °C.

Analogous phase composition studies were performed for binary CeO₂–Al₂O₃ systems containing different contents of CeO₂. The analysis showed that in parallel to the CeO₂ content increase in the binary oxide system, the main peak of the CeO₂ fluorite structure became sharper and stronger indicating that this oxide is better crystallized on the aluminium oxide surface [53]. No further phases were observed in the diffraction patterns recorded for other binary oxide systems.

To study the changes of the phase composition during the activation process performed before the catalytic tests and to explain the reduction behaviour of the mono- and bimetallic catalysts supported on binary oxide, in situ XRD measurements in a mixture of 5% H₂–95% Ar were carried out in the temperature range of 50–500 °C for bimetallic catalysts supported on mono Al₂O₃, CeO₂, and binary oxide CeO₂–Al₂O₃. Bimetallic Pd–Ni/CeO₂ catalyst was first tested. Results are given in Figure 4. The analysis of the diffraction curves recorded for bimetallic Pd–Ni catalyst supported on CeO₂ showed that from 50 °C to 250 °C the diffraction curves showed only NiO and CeO₂ phases. Increase in the reduction temperature above 250 °C results in disappearance of the NiO phase. The X-ray Powder Diffraction (XRD) pattern recorded at 300 °C for Pd–Ni/CeO₂ catalyst showed the diffraction

peaks of metallic nickel and CeO_2 phases. Further increase in the reduction temperature above 300 °C caused the appearance of CeO_2 and metallic nickel phases in the diffraction curves. In the next step of the XRD, in situ measurements, Pd–Ni/ Al_2O_3 bimetallic supported catalysts were studied and the diffraction curves obtained in the investigated temperature range are presented in Figure 5.

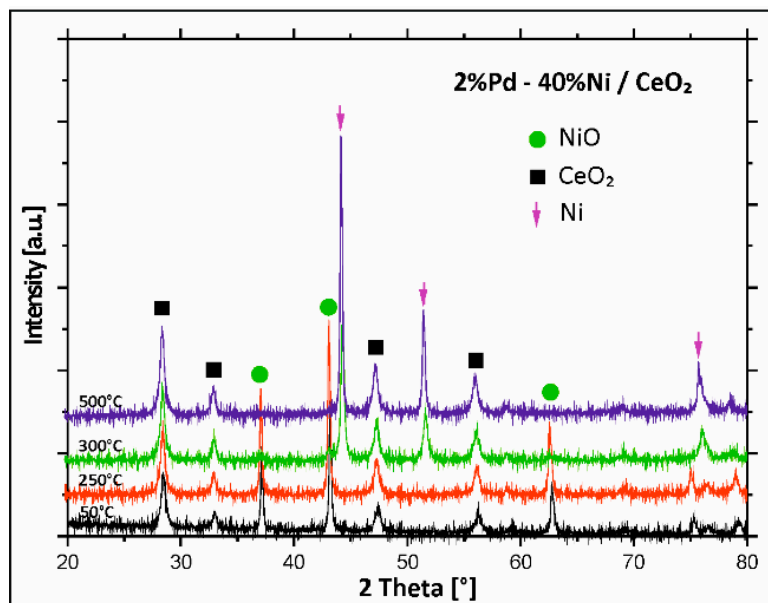


Figure 4. X-ray powder patterns recorded during reduction of calcined bimetallic Pd–Ni/ CeO_2 catalyst in a mixture of 5% H_2 –95%Ar in the temperature range 50–500 °C.

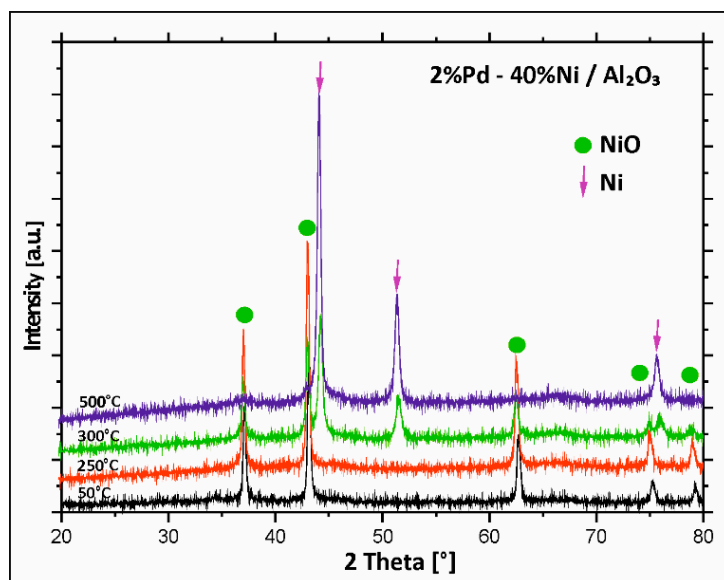


Figure 5. X-ray powder patterns recorded during reduction of calcined bimetallic Pd–Ni/ Al_2O_3 catalyst in a mixture of 5% H_2 –95%Ar in the temperature range 50–500 °C.

Analogous measurements were performed in the same temperature range for Pd–Ni/ Al_2O_3 catalyst. At the starting temperature of 50 °C, the diffraction pattern showed the existence of a NiO phase. At 300 °C, additional metallic nickel phase was detected in the diffraction curve. Increasing the reduction temperature above 300 °C showed the disappearance of the diffraction peaks assigned to the NiO phase. At the final reduction temperature of 500 °C only the metallic nickel phase was detected. The lack of the γ - Al_2O_3 is explained by the high amorphousness of this phase.

Figure 6 presents the phase composition studies performed for Pd–Ni/CeO₂–Al₂O₃ catalyst. The analysis of the X-ray diffraction measurements performed for bimetallic catalysts supported on binary oxide CeO₂–Al₂O₃ showed the existence of NiO and CeO₂ phases at temperature below 250 °C. The increase in the activation process temperature to 300 °C results in appearance of an additional metallic nickel phase. Further temperature increase above 300 °C, causes disappearance of the diffraction peaks assigned to the NiO phase and the presence of reflexes originating from metallic Ni and CeO₂ phases. Summarizing, the, in situ X-ray diffraction measurements performed for all bimetallic catalysts in a temperature range of 50–500 °C confirmed the proposed reduction mechanism of NiO species described above for mono- and bimetallic Pd–Ni catalyst supported on CeO₂–Al₂O₃ binary oxide. The results support two steps of nickel (II) oxide reduction through a reduction of unbound and interaction with the carrier NiO species. In addition, it should be also emphasized, that the metallic Pd phase was not visible on the diffraction curves recorded for all bimetallic supported catalysts. The lack of the diffraction peaks assigned to the metallic Pd phase in the diffraction curves means that Pd particles have too small a size to be detected by XRD technique.

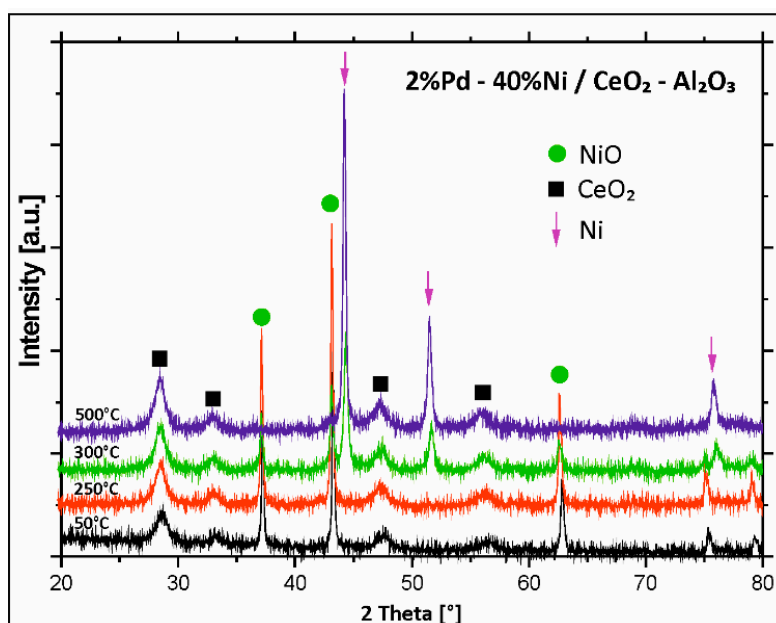


Figure 6. X-ray powder patterns recorded during reduction of calcined bimetallic Pd–Ni/CeO₂–Al₂O₃ catalyst in a mixture of 5%H₂–95%Ar in the temperature range 50–500 °C.

2.5. Temperature Programmed Desorption of Ammonia TPD–NH₃

The total acidity and the distribution of acid centres calculated based on the area under the peak situated at an appropriate desorption temperature of the prepared catalysts were studied using temperature-programmed desorption of ammonia. TPD–NH₃ experiments were performed in order to elucidate the influence of Ni and Pd on the acidity of the prepared systems and to determine the role of their acidity on the catalytic activity in the process of oxy-steam reforming of methanol. It is well known that the acidity centres play a crucial role during reforming of methanol.

The acidity centres are involved in the stabilization of intermediates formed during reforming of methanol. The rate and amount of the formed intermediates such as: methoxy, formate, and carbonate species significantly affect the catalytic activity of the studied systems in oxy-steam reforming of methanol. The results of the surface acidity obtained for all investigated catalytic systems are given in Table 3 and Figure 7. TPD–NH₃ measurements performed over support material as well as monometallic and bimetallic supported catalysts indicated that the total surface acidity of all studied systems was in the range of 0.26–0.63 mmol NH₃·g^{−1}_{cat}. Binary oxide itself showed a total acidity of 0.59 mmol·g^{−1}_{cat}. The introduction of a small amount of nickel into the support surface results

in a slight increase of the total acidity of the formed catalyst. Further increase in the metal content causes decrease in surface acidity. The lowest total acidity amongst all nickel catalysts supported on $\text{CeO}_2\text{-Al}_2\text{O}_3$ was shown to be the 40% Ni/ $\text{CeO}_2\text{-Al}_2\text{O}_3$ catalyst. In contrast, comparison of the acidity of nickel catalysts supported on mono- Al_2O_3 or CeO_2 and binary oxide $\text{CeO}_2\text{-Al}_2\text{O}_3$ showed that the highest acidity was exhibited by the Ni/ Al_2O_3 catalyst. The lowest value of total ammonia desorbed from the catalyst surface was shown to be the Ni/ CeO_2 system while the 40%Ni/ $\text{CeO}_2\text{-Al}_2\text{O}_3$ had an intermediate total acidity value. Total acidity of the nickel catalysts supported on aluminium oxide and ceria–alumina oxides were also measured by $\text{NH}_3\text{-TPD}$ by Reyes et al. [52]. The results of the acidity showed that high addition of Ce (>10 wt%) caused a decrease in the total acidity. The authors reported that CeO_2 introduction into the $\gamma\text{-Al}_2\text{O}_3$ mono-oxide reduces the amount and strength of the acidic sites. The acidity of the nickel supported catalysts was also studied by Jiao et al. [54]. All of the supported nickel catalysts showed, as in our case, three or four strong desorption peaks in the temperature range of 100–500 °C. It is also worth mentioning that the largest desorption peaks contain the weak and medium acid centres. The authors also obtained similar results. They found that the amount of acid centres decreases parallel to the addition of metal Ni. The catalytic activity is dependent on the acidity of the system and the strength of the acidic centres present in the tested catalyst. The process of the oxy-steam reforming of methanol was carried out at temperatures of up to 250 °C which can mean that medium-strength and strong acid sites are blocked by strongly adsorbed reaction species and are not available for adsorption of methanol in the low temperature range. The acidity results obtained for the investigated catalysts indicate that the catalytic systems exhibited acidity in the temperature range of 100–300 °C and 0.07–0.13 mmol of desorbed ammonia per gram of catalyst. It should be also noted that poorly active systems such as 5%Ni/ $\text{CeO}_2\text{-Al}_2\text{O}_3$ and 20%Ni/ Al_2O_3 showed the highest values of acidity equal to 0.12 and 0.13 mmol/g cat., respectively. This means that some limited acidity is required to achieve highly active systems in the studied process. Too high values of acid centres have a negative impact on the catalytic activity. Too many acid centres lead to methanol decomposition to methoxy and methyl groups, eventually leading to dimethyl ether formation (see Table 1).

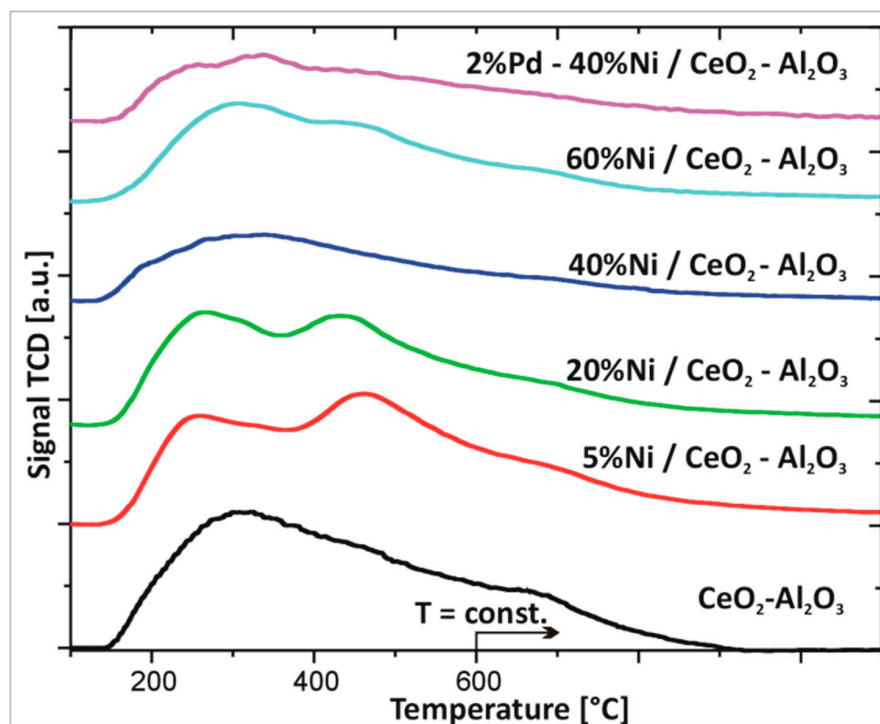


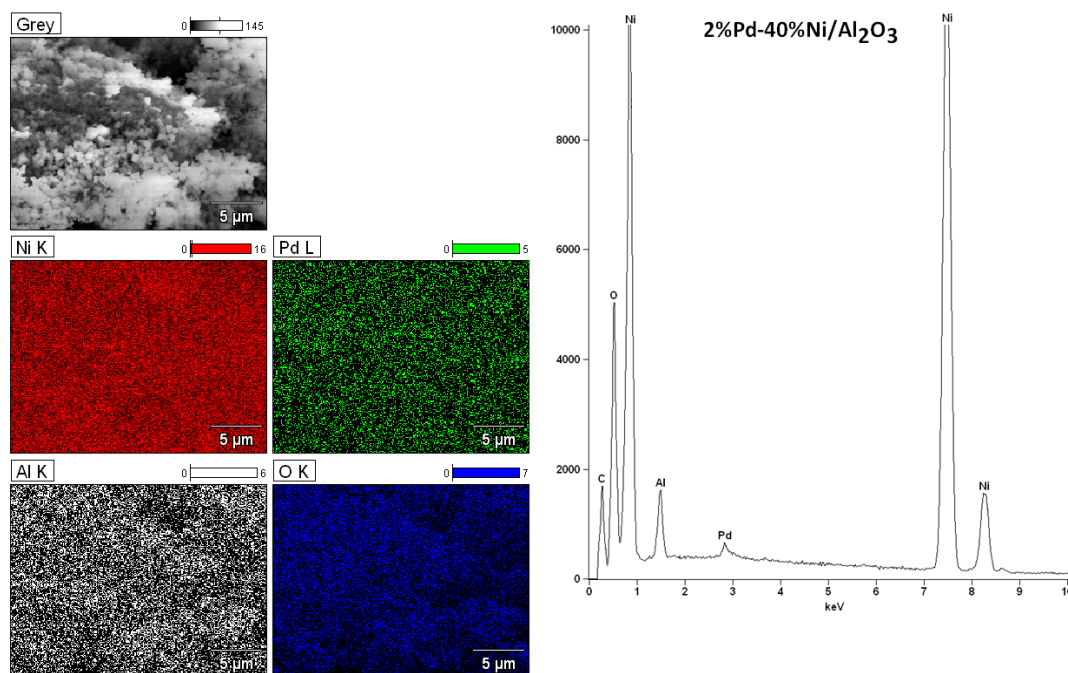
Figure 7. TPD- NH_3 profile of the binary oxide and monometallic catalysts after calcination in air for 4 h at 400 °C.

Table 3. The amount of NH_3 adsorbed on supports, monometallic nickel and bimetallic Pd–Ni/ CeO_2 – Al_2O_3 catalysts calcined in air atmosphere at 400 °C from the TPD– NH_3 data.

Catalysts/Supports	Weak Centres (mmol/g) 100–300 °C	Medium Centres (mmol/g) 300–450 °C	Strong Centres (mmol/g) 450–600 °C	Total Acidity (mmol/g) 100–600 °C
CeO_2 – Al_2O_3	0.13	0.19	0.27	0.59
5%Ni/ CeO_2 – Al_2O_3	0.12	0.17	0.34	0.63
20%Ni/ CeO_2 – Al_2O_3	0.12	0.16	0.28	0.56
40%Ni/ CeO_2 – Al_2O_3	0.07	0.10	0.13	0.30
60%Ni/ CeO_2 – Al_2O_3	0.09	0.14	0.18	0.41
40%Ni/ CeO_2	0.07	0.07	0.12	0.26
40%Ni/ Al_2O_3	0.13	0.15	0.24	0.52
2%Pd–40%Ni/ CeO_2 – Al_2O_3	0.06	0.09	0.13	0.28

2.6. Morphology Studies of Mono and Bimetallic Supported Catalysts Using SEM–EDS

The morphology and the elemental composition of the bimetallic 2%Pd–40%Ni catalysts supported on mono- Al_2O_3 , CeO_2 and binary oxide CeO_2 – Al_2O_3 were extensively studied by a scanning electron microscope (SEM), equipped with an energy dispersive spectrometer (EDS). The results of the scanning electron microscope-energy dispersive spectrometer (SEM-EDS) measurements performed for bimetallic catalyst supported on aluminium oxide calcined at 400 °C are given in Figure 8.

**Figure 8.** scanning electron microscope (SEM) images and energy dispersive spectrometer (EDS) spectra for the bimetallic 2%Pd–40%Ni/ Al_2O_3 catalysts calcined at 400 °C in air atmosphere for 4 h.

The magnification during the analysis of bimetallic catalytic system was 5000. The surface analysis performed for bimetallic catalyst showed the occurrence of nickel, aluminium, oxygen and palladium on the catalytic surface. Figure 9 presents the analogous measurements carried out for bimetallic catalyst supported on CeO_2 after calcination at 400 °C in air atmosphere. The EDS spectrum collected from the surface confirmed the presence of nickel, cerium, and oxygen. The lack of palladium would suggest covering of this element by other catalyst components on the catalyst surface. In order to investigate the elemental composition of the catalyst, the same measurements were performed for bimetallic catalyst supported on binary oxide. The surface analysis of bimetallic Pd–Ni/ CeO_2 – Al_2O_3

catalyst calcined at 400 °C in air showed similar results (see Figure 10). The only difference was the presence of aluminium on the catalyst surface. Additionally, the regions on which cerium and aluminium elements are present can be easily distinguished. This result can be explained by a specific interaction between CeO₂ and Al₂O₃ oxides and could be confirmed by the reduction results obtained for the systems supported on CeO₂–Al₂O₃ binary oxide.

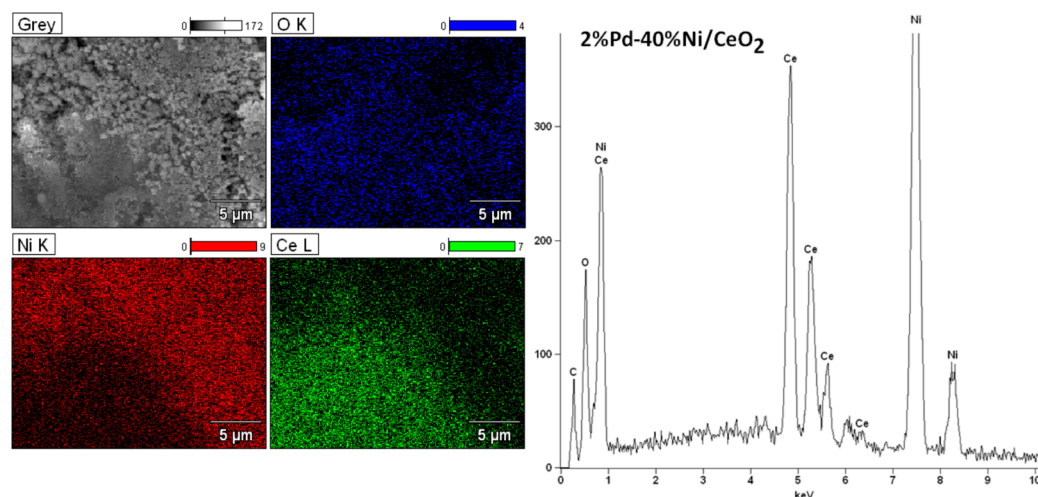


Figure 9. SEM images and EDS spectra for the bimetallic 2%Pd–40%Ni/CeO₂ catalysts calcined at 400 °C in air atmosphere for 4 h.

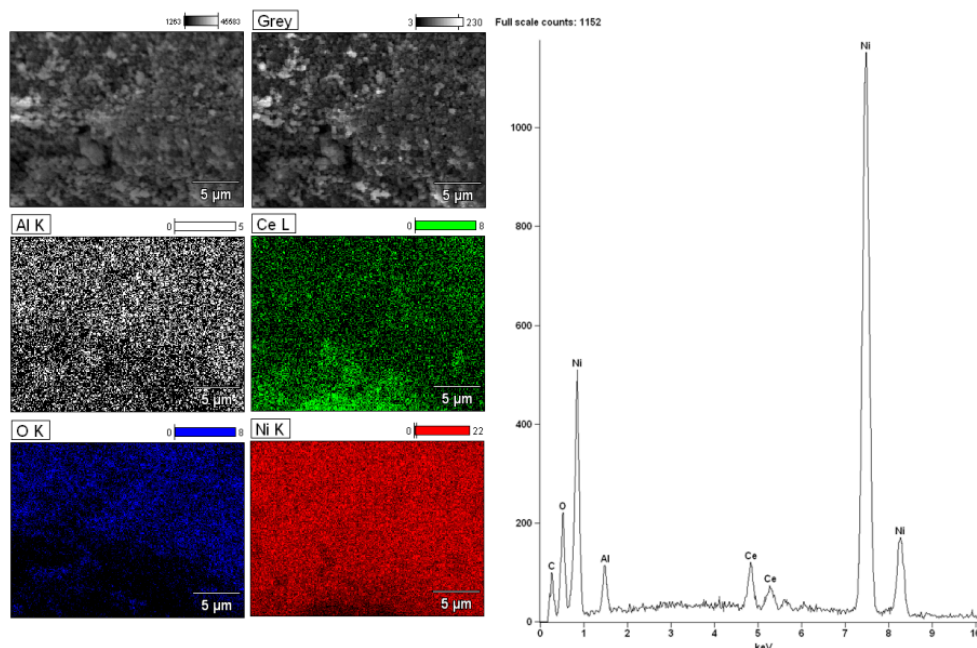


Figure 10. SEM images and EDS spectra for the bimetallic 2%Pd–40%Ni/CeO₂–Al₂O₃ catalysts calcined at 400 °C in air atmosphere for 4 h.

2.7. Interaction between the Active Phase Component and Support

X-ray photoelectron spectroscopy (XPS) was used to study the electronic structure and the chemical surface composition of the catalytic material. This technique is a very powerful method to study the changes in the electronic structure of the active phase component supported on various support surfaces. In this work, the electronic structural changes of Ni after promotion of monometallic nickel catalyst by palladium were investigated.

In order to elucidate the interaction between the active phase component and/or support the X-ray photoelectron spectroscopy analysis was carried out for monometallic Ni and bimetallic 2%Pd–40%Ni/CeO₂–Al₂O₃ after reduction in a mixture of 5%H₂–95%Ar at 500 °C. The XPS high resolution spectra of the binding energies between 844 and 884 eV show several characteristic peaks (see Figure 11). The peak in the region of 844–884 eV includes Ni²⁺ species (859 eV) and metallic nickel (856 eV). The typical position of the XPS bands which supports the presence of Ni²⁺ and Ni⁰ in the sample is 856 and 852.8 eV, respectively. The shift of the observed band assigned to the Ni²⁺ towards higher binding energy indicates that most of the nickel is in its oxidized or charged states. For our investigated catalysts the observed shifts of the specific bands are connected with the interaction which take place between NiO and Al₂O₃ or CeO₂ monoxides. This result confirmed the observed reduction profiles on the TPR–H₂ curves recorded for monometallic and bimetallic catalysts supported on the CeO₂–Al₂O₃ binary oxide system. Luisetto et al. [55] studied Ni catalysts supported on the CeO₂–Al₂O₃ system by XPS. They reported complicated Ni 2p spectra due to the presence of high binding energy satellites. The calcined sample showed the main peak positioned at a binding energy of 854 eV which was attributed to the Ni²⁺ species. The shift of this peak related to the typical signal positioned at 856 was explained by the high interaction with the support. The XPS analysis performed by the authors for reduced catalyst showed the characteristic band assigned to the metallic nickel at lower binding energy values of Ni 2p_{3/2} = 853.0–853.5 eV. The observed shift can be associated with the partial oxidation of the sample before the real measurement.

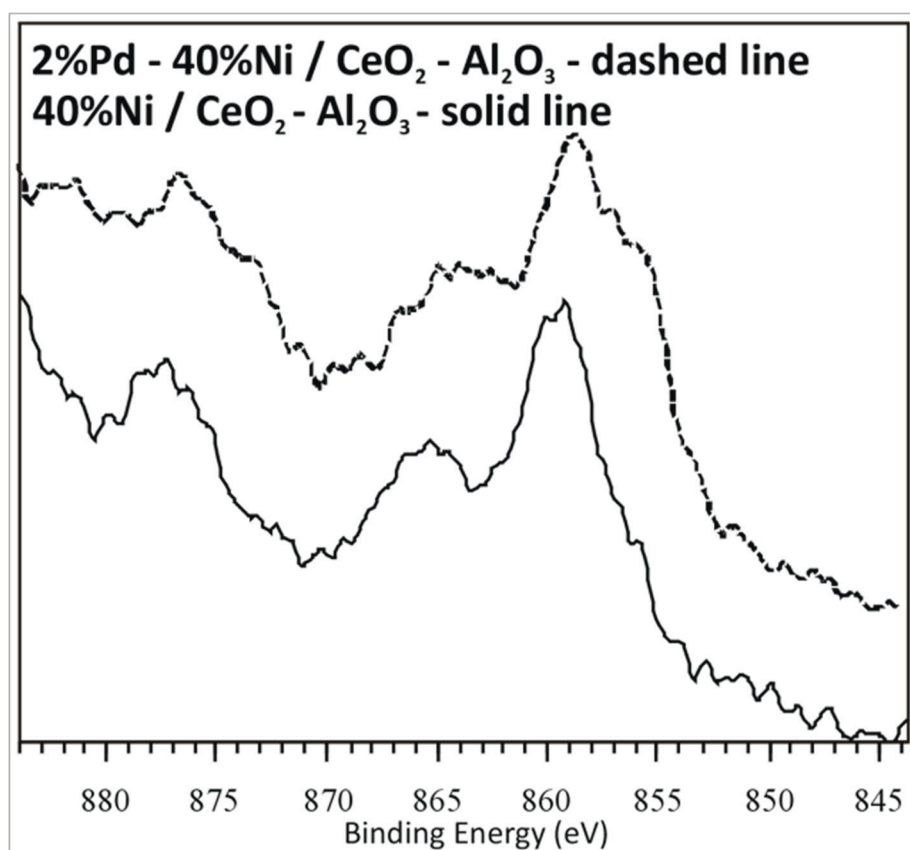


Figure 11. Ni 2p X-ray photoelectron spectroscopy (XPS) spectra of 40%Ni/CeO₂–Al₂O₃ and 2%Pd–40%Ni/CeO₂–Al₂O₃ reduced in a mixture of 5%H₂–95%Ar at 500 °C.

3. Experimental

3.1. Catalytic Material Preparation

3.1.1. Support Material

Monoxides such as Al_2O_3 or CeO_2 were prepared by a precipitation method using ammonia as a precipitation agent. The resulting solid obtained after precipitation process was aged for 12 h. Then final precipitates were washed twice in deionized water and dried at 120 °C for 15 h in an air atmosphere. Finally, the obtained supports were calcined in air atmosphere for 4 h at 400 °C.

The CeO_2 – Al_2O_3 support with a Ce Al molar ratio of 1:2 was prepared by a precipitation method. Aluminium and cerium nitrates were used during the co-precipitation step. A concentrated ammonia solution was used as a precipitation agent and was added dropwise until the pH reached values between 10 and 11. Then, the resulting mixtures were stirred for another 30 min. The resulting precipitate was aged for 12 h and after that it was washed twice in deionized water, dried at 120 °C for 15 h, and calcined in air for 4 h at 400 °C.

3.1.2. Preparation of Supported Monometallic and Bimetallic Catalysts

Nickel supported catalysts were prepared by a conventional wet aqueous impregnation method. NiO phase was introduced on the support (CeO_2 – Al_2O_3 , CeO_2 , Al_2O_3) surface by a wet impregnation method from the nickel nitrate (V) aqueous solutions. Then the obtained systems were dried for 2 h at 120 °C in an air atmosphere and finally calcined for 4 h in air atmosphere at 400 °C. Palladium phase was introduced on the Ni/support catalysts surface by a consequent impregnation method using $\text{Pd}(\text{NO}_3)_2$ solution. Then the bimetallic systems were dried for 2 h in air atmosphere at 120 °C, and then calcined at 400 °C for 4 h at the same atmosphere. Nickel and palladium contents in the catalytic material were 5, 20, 40, and 60 wt% of Ni and 2 wt% of Pd, respectively.

3.2. Catalytic Material Characterization

The BET surface area and porosity of the catalytic materials were determined in a sorptometer Sorptomatic 1900 apparatus. Reducibility of the prepared catalysts studied by temperature-programmed-reduction measurements were carried out in an automatic AMI-1 instrument (Altamira Instruments, Pittsburgh, PA, USA) in the temperature range of 25–900 °C with a heating rate of 10 °C min^{−1}. The mass of the sample in each test was ~0.1 g. The investigated materials were reduced in a mixture of 5% H_2 –95% Ar with a volumetric flow rate of 40 cm³/min. Hydrogen consumption was measured using a thermal conductivity detector. Phase composition studies of the catalysts were studied using a PANalytical X'Pert Pro MPD diffractometer (Malvern Panalytical Ltd., Royston, UK) in Bragg–Brentano reflecting geometry. $\text{CuK}\alpha$ radiation from a sealed tube was applied during all measurements. Obtained data were collected at the 2 θ angle 5–90°. All calculations during analysis were carried out using X'PertHighScore Plus computer software (ver. 3.0e, Malvern Panalytical Ltd., Royston, UK, 2012). In addition, the phase composition studies of the selected Pd–Ni bimetallic catalysts during the reduction in a mixture of a 5% H_2 –95% Ar in the temperature range 50–500 °C were carried out in a PANalytical X'Pert Pro diffractometer equipped with an Anton Paar XRK900 reactor chamber (Anton Paar, Graz, Austria). During each measurement a PANalytical X'Celerator detector based on Real Time Multiple Strip technology was used. The acidity of the prepared catalysts was studied by TPD– NH_3 technique. All TPD– NH_3 experiments were done using homemade apparatus. Prior to each measurement the sample surface was previously purified in flowing He at 600 °C for 60 min. Then the NH_3 was adsorbed on the catalyst surface at 50 °C for 30 min. Afterwards, the physically adsorbed NH_3 was removed from the surface in a helium stream at 100 °C. Then in the next step, the chemically adsorbed NH_3 on the catalyst surface was determined using a temperature programmed desorption process in the temperature range 100–600 °C with a heating rate of 25 °C min^{−1}. A thermal-conductivity detector was used to monitor the concentration of the

chemically desorbed ammonia from the surface of the investigated sample. Hydrogen chemisorption measurements were performed in a Micromeritics ASAP 2020 apparatus (Micromeritics, Norcross, GA, USA). Before the appropriate H₂ chemisorption process, each catalytic material was reduced in situ at 500 °C in a mixture of 5% H₂–95% Ar for 2 h. Then the samples were cooled to 35 °C under inert gas (He). In the following step the amount of the chemisorbed hydrogen was determined using the adsorption–backdesorption isotherm method. The Scanning Electron Microscope (S-4700 HITACHI, Tokyo, Japan) equipped with EDX detector (ThermoNoran, Madison, WI, USA) was used to measure the surface morphology of the selected micro-area of the bimetallic catalysts. The surface analysis was carried out at several magnifications. Qualitative analysis of the micro-area of the sample surface layer was carried out based on the X-ray spectra. The distributions of each element on the studied micro-area were analysed. The accelerating voltage applied during the investigations was 25 kV. A Specs SAGE XPS spectrometer (SPECS GmbH, Germany) was used to study the electronic structure of the active phase component. For the analysis powder of the sample was attached to carbon tape. The spectrometer was operated at 10 kV and 20 mA using Mg K α radiation source ($h = 1253.6$ eV) in each measurement. The high resolution (0.1 eV) spectra were then recorded for pertinent photoelectron peaks at a pass energy of 20 eV to identify the chemical state of each element. The analyzed area was circular with a diameter of 5 mm. Charge compensation of the spectra was done based on the position of the aliphatic carbon peak which was set at 285 eV. The high-resolution spectra were analysed using CasaXPS software (Casa Software Ltd., Andover, MA, USA).

3.3. Catalytic Activity Evaluation

The oxy-steam reforming of the methanol process was carried out using a flow quartz micro-reactor under atmospheric pressure at a temperature of 200 and 250 °C, respectively. The composition of the reaction mixture used in each catalytic test was as follows H₂O/CH₃OH/O₂ = 1/1/0.4 (molar ratio) and the GHSV was 26,700 h^{−1} (calculated at ambient temperature and under atmospheric pressure). The total flow-rate was kept at 31.5 mL/min and the Ar was used as the balance gas (the methanol content in the reaction mixture was 6%). The reaction mixture was prepared using two saturators. One was used to saturate argon in methanol vapour and the second one was used to saturate the mixture of 5% O₂–95% Ar in steam. The flow of the mixed gases was controlled by flow meters. Before introduction into the micro-reactor both gases were mixed. The reaction mixture leaving the micro-reactor was directed to the first GC equipped with Flame Ionisation Detector (FID) where the methanol conversion and the concentration of other organics compounds were evaluated. Then the mixture was passed through the steam trap and directed to the second and third GC where hydrogen and other products (CO, CO₂) were monitored, respectively [1]. The activity measurements were taken after two hours of stabilization at each temperature. The mass of the catalyst used in each test was 0.2 g [1]. The analysis of the reaction organic products (methanol, methane, methyl formate, dimethylether (DME), and formaldehyde) was carried out by an on-line gas chromatograph equipped with FID detector and 10% Carbowax 1500 on a Graphpac column. While, CO and CO₂ concentrations were followed by a GC chromatograph equipped with a Thermal Conductivity Detector (TCD) (150 °C, 60 mA), and Carbosphere 60/80 (50 °C) column. The hydrogen concentration was measured by a GC chromatograph equipped with TCD detector (120 °C, 60 mA) and molecular sieve 5a (120 °C) column. In each experiment material balances on carbon were calculated to verify the obtained results. The selectivity results for all catalysts towards the formation of hydrogen, carbon monoxide, carbon dioxide, and DME in OSRM was calculated using Equations (1)–(4) and the conversion of methanol using Equation (5):

$$S_{H_2}(\%) = \frac{(n_{H_2-out})}{\sum \text{products of the reaction}} * 100 \quad (1)$$

$$S_{CO}(\%) = \frac{(n_{CO-out})}{\sum \text{products of the reaction}} * 100 \quad (2)$$

$$S_{\text{CO}_2}(\%) = \frac{(n_{\text{CO}_2\text{-out}})}{\sum \text{products of the reaction}} * 100 \quad (3)$$

$$S_{\text{DME}}(\%) = \frac{(n_{\text{DME}_{\text{out}}})}{\sum \text{products of the reaction}} * 100 \quad (4)$$

where, $n_{\text{CH}_3\text{OH}}$ and n_{H_2} is the molar flow rate of CH_3OH and H_2 , respectively.

$$\text{Conv.}_{\text{CH}_3\text{OH}}(\%) = \frac{n_1^{\text{in}}\text{CH}_3\text{OH} - n_2^{\text{out}}\text{CH}_3\text{OH}}{n_1^{\text{in}}\text{CH}_3\text{OH}} * 100 \quad (5)$$

where,

$n_{\text{H}_2\text{-out}}$ -molar flow rate of H_2 feed out,

$n_{\text{CO}_2\text{-out}}$ -molar flow rate of CO_2 feed out,

$n_{\text{CO}_{\text{out}}}$ -molar flow rate of CO feed out,

$n_1^{\text{in}} \text{CH}_3\text{OH}$, $n_2^{\text{out}} \text{CH}_3\text{OH}$ -molar flow rate of CH_3OH feed in and feed out, respectively.

Methane, formaldehyde, and methyl formate formation were not observed. Only carbon monoxide, carbon dioxide, hydrogen, and DME were formed as reaction products during the process.

4. Conclusions

In summary, monometallic $\text{Ni/CeO}_2\text{-Al}_2\text{O}_3$ and bimetallic $\text{Pd-Ni/CeO}_2\text{-Al}_2\text{O}_3$ catalysts were prepared by an impregnation and subsequent impregnation method, respectively. The oxy-steam reforming of the methanol reaction was successfully carried out for monometallic Ni and bimetallic Pd-Ni catalysts supported on the binary oxide $\text{CeO}_2\text{-Al}_2\text{O}_3$ system for hydrogen production. The catalytic activity results performed for all catalysts showed that bimetallic $2\%\text{Pd-}40\%\text{Ni/CeO}_2\text{-Al}_2\text{O}_3$ catalyst exhibit the highest activity and stability as well as the highest selectivity towards hydrogen formation in the OSRM process. The reactivity results confirmed the promotion effect of palladium on the catalyst activity of Ni supported catalyst. It was also proven that palladium facilitates the reduction of NiO species on the catalyst surface by the spill over effect occurring between Pd and NiO . The facilitated reduction of NiO species and the generation of additional adsorption centres on the catalyst surface after the introduction of palladium may be responsible for increasing the catalytic activity and selectivity of the bimetallic catalyst towards hydrogen formation. The performed measurements showed that the activity results strongly depend on the content of nickel, their acidity, and their reducibility. The experimental results confirmed that both metal active centres and acid sites play a crucial role during oxy-steam reforming of methanol. In addition, the acid centres located close to the high dispersed metal centres may have a significant effect on the catalytic activity of the investigated catalyst. The activity measurements showed that the synthesized palladium-nickel system exhibited high stability in the OSRM process which confirms their potential use in fuel cell technology.

Author Contributions: Data curation, P.M.; Investigation, P.M., A.M., M.M., R.C., W.M., M.N. and K.V.; M.N. performed chemisorption measurements, W.M. performed XRD measurements, R.C. performed activity tests, TPR and TPD experiments, Methodology, P.M.; K.V. and A.M. performed and analyzed XPS measurements, Research consultation, M.I.S., A.C., Analysis of the SEM-EDS measurements, M.I.S., Project administration, P.M.; Supervision, P.M. and M.I.S.; Visualization, P.M., A.C. and M.M.; Writing-original draft, P.M.; Writing-review & editing, P.M.

Funding: This work was funded by Polish Ministry of Science and Higher Education within the “*Iuventus Plus*” Programme (2015–2017) (project No. 0305/IP2/2015/73).

Acknowledgments: I would like to thank A. Kedziora for help in the research (TPR- H_2 , TPD- NH_3 , activity tests) carried out in the framework of the work.

Conflicts of Interest: The authors declare no conflict of interest.

References

1. Mierczynski, P.; Vasilev, K.; Mierczynska, A.; Maniukiewicz, W.; Szyrkowska, M.I.; Maniecki, T.P. Bimetallic Au–Cu, Au–Ni catalysts supported on MWCNTs for oxy-steam reforming of methanol. *Appl. Catal. B Environ.* **2016**, *185*, 281–294. [[CrossRef](#)]
2. Voloshin, R.A.; Rodionova, M.V.; Zharmukhamedov, S.K.; Veziroglu, T.N.; Allakhverdiev, S.I. Review: Biofuel production from plant and algal biomass. *Int. J. Hydrog. Energy* **2016**, *41*, 17257–17273. [[CrossRef](#)]
3. Bae, J.; Lee, S.; Kim, S.; Oh, J.; Choi, S.; Bae, M.; Kang, I.; Katikaneni, S.P. Liquid fuel processing for hydrogen production: A review. *Int. J. Hydrog. Energy* **2016**, *41*, 19990–20022. [[CrossRef](#)]
4. Mierczynski, P.; Vasilev, K.; Mierczynska, A.; Ciesielski, R.; Maniukiewicz, W.; Rogowski, J.; Szyrkowska, I.M.; Trifonov, A.Y.; Dubkov, S.V.; Gromov, D.; et al. The effect of gold on modern bimetallic Au–Cu/MWCNT catalysts for oxy-steam reforming of methanol. *Catal. Sci. Technol.* **2016**, *6*, 4168–4183. [[CrossRef](#)]
5. Lu, J.; Li, X.; He, S.; Han, C.; Wan, G.; Lei, Y.; Chen, R.; Liu, P.; Chen, K.; Zhang, L.; et al. Hydrogen production via methanol steam reforming over Ni-based catalysts: Influences of Lanthanum (La) addition and supports. *Int. J. Hydrog. Energy* **2017**, *42*, 3647–3657. [[CrossRef](#)]
6. Mierczynski, P.; Ciesielski, R.; Kedziora, A.; Nowosielska, M.; Kubicki, J.; Maniukiewicz, W.; Czyrkowska, A.; Maniecki, T. Monometallic copper catalysts supported on multi-walled carbon nanotubes for the oxy-steam reforming of methanol. *React. Kinet. Mech. Catal.* **2016**, *117*, 675–691. [[CrossRef](#)]
7. Liu, X.; Toyir, J.; de la Piscina, P.R.; Homs, N. Hydrogen production from methanol steam reforming over Al₂O₃- and ZrO₂-modified CuO/ZnO/Ga₂O₃ catalysts. *Int. J. Hydrog. Energy* **2017**, *42*, 13704–13711. [[CrossRef](#)]
8. Mierczynski, P.; Vasilev, K.; Mierczynska, A.; Maniukiewicz, W.; Maniecki, T.P. Highly selective Pd–Cu/ZnAl₂O₄ catalyst for hydrogen production. *Appl. Catal. A Gen.* **2014**, *479*, 26–34. [[CrossRef](#)]
9. Liu, D.; Men, Y.; Wang, J.; Kolb, G.; Liu, X.; Wang, Y.; Sun, Q. Highly active and durable Pt/In₂O₃/Al₂O₃ catalysts in methanol steam reforming. *Int. J. Hydrog. Energy* **2016**, *41*, 21990–21999. [[CrossRef](#)]
10. Mierczynski, P.; Vasilev, K.; Mierczynska, A.; Maniukiewicz, W.; Maniecki, T. The Effect of ZnAl₂O₄ on the Performance of Cu/Zn_xAl_yO_{x+1.5y} Supported Catalysts in Steam Reforming of Methanol. *Top. Catal.* **2013**, *56*, 1015–1025. [[CrossRef](#)]
11. Luo, Z.; Li, D.; Tang, H.; Pan, M.; Ruan, R. Degradation behavior of membrane-electrode-assembly materials in 10-cell PEMFC stack. *Int. J. Hydrog. Energy* **2006**, *31*, 1831–1837. [[CrossRef](#)]
12. Xu, H.; Hou, X. Synergistic effect of CeO₂ modified Pt/C electrocatalysts on the performance of PEM fuel cells. *Int. J. Hydrog. Energy* **2007**, *32*, 4397–4401. [[CrossRef](#)]
13. Mierczynski, P. Comparative Studies of Bimetallic Ru–Cu, Rh–Cu, Ag–Cu, Ir–Cu Catalysts Supported on ZnO–Al₂O₃, ZrO₂–Al₂O₃ Systems. *Catal. Lett.* **2016**, *146*, 1825–1837. [[CrossRef](#)]
14. López, P.; Mondragón-Galicia, G.; Espinosa-Pesqueira, M.E.; Mendoza-Anaya, D.; Fernández, M.E.; Gómez-Cortés, A.; Bonifacio, J.; Martínez-Barrera, G.; Pérez-Hernández, R. Hydrogen production from oxidative steam reforming of methanol: Effect of the Cu and Ni impregnation on ZrO₂ and their molecular simulation studies. *Int. J. Hydrog. Energy* **2012**, *37*, 9018–9027. [[CrossRef](#)]
15. Mierczynski, P.; Mierczynska, A.; Maniukiewicz, W.; Maniecki, T.P.; Vasilev, K. MWCNTs as a catalyst in oxy-steam reforming of methanol. *RSC Adv.* **2016**, *6*, 81408–81413. [[CrossRef](#)]
16. Chang, C.-C.; Chang, C.-T.; Chiang, S.-J.; Liaw, B.-J.; Chen, Y.-Z. Oxidative steam reforming of methanol over CuO/ZnO/CeO₂/ZrO₂/Al₂O₃ catalysts. *Int. J. Hydrog. Energy* **2010**, *35*, 7675–7683. [[CrossRef](#)]
17. Chang, C.-C.; Hsu, C.-C.; Chang, C.-T.; Chen, Y.-P.; Liaw, B.-J.; Chen, Y.-Z. Effect of noble metal on oxidative steam reforming of methanol over CuO/ZnO/Al₂O₃ catalysts. *Int. J. Hydrog. Energy* **2012**, *37*, 11176–11184. [[CrossRef](#)]
18. Pérez-Hernández, R.; Gutiérrez-Martínez, A.; Gutiérrez-Wing, C.E. Effect of Cu loading on for hydrogen production by oxidative steam reforming of methanol. *Int. J. Hydrog. Energy* **2007**, *32*, 2888–2894. [[CrossRef](#)]
19. Sá, S.; Silva, H.; Brandão, L.; Sousa, J.M.; Mendes, A. Catalysts for methanol steam reforming—A review. *Appl. Catal. B Environ.* **2010**, *99*, 43–57. [[CrossRef](#)]
20. Pérez-Hernández, R.; Gutiérrez-Martínez, A.; Espinosa-Pesqueira, M.E.; Estanislao, M.L.; Palacios, J. Effect of the bimetallic Ni/Cu loading on the ZrO₂ support for H₂ production in the autothermal steam reforming of methanol. *Catal. Today* **2015**, *250*, 166–172. [[CrossRef](#)]

21. Yong, S.T.; Ooi, C.W.; Chai, S.P.; Wu, X.S. Review of methanol reforming-Cu-based catalysts, surface reaction mechanisms, and reaction schemes. *Int. J. Hydrog. Energy* **2013**, *38*, 9541–9552. [[CrossRef](#)]
22. Pérez-Hernández, R.; Galicia, G.M.; Anaya, D.M.; Palacios, J.; Angeles-Chavez, C.; Arenas-Alatorre, J. Synthesis and characterization of bimetallic Cu–Ni/ZrO₂ nanocatalysts: H₂ production by oxidative steam reforming of methanol. *Int. J. Hydrog. Energy* **2008**, *33*, 4569–4576. [[CrossRef](#)]
23. Yang, H.-M.; Chan, M.-K. Steam reforming of methanol over copper–yttria catalyst supported on praseodymium–aluminum mixed oxides. *Catal. Commun.* **2011**, *12*, 1389–1395. [[CrossRef](#)]
24. Perez-Hernandez, R.; Mondragon-Galicia, G.; Maravilla, A.A.; Palacios, J. Nano-dimensional CeO₂ nanorods for high Ni loading catalysts: H₂ production by autothermal steam reforming of methanol reaction. *Phys. Chem. Chem. Phys.* **2013**, *15*, 12702–12708. [[CrossRef](#)] [[PubMed](#)]
25. Turco, M.; Bagnasco, G.; Cammarano, C.; Senese, P.; Costantino, U.; Sisani, M. Cu/ZnO/Al₂O₃ catalysts for oxidative steam reforming of methanol: The role of Cu and the dispersing oxide matrix. *Appl. Catal. B Environ.* **2007**, *77*, 46–57. [[CrossRef](#)]
26. Pojanavaraphan, C.; Satitthai, U.; Luengnaruemitchai, A.; Gulari, E. Activity and stability of Au/CeO₂–Fe₂O₃ catalysts for the hydrogen production via oxidative steam reforming of methanol. *J. Ind. Eng. Chem.* **2015**, *22*, 41–52. [[CrossRef](#)]
27. Turco, M.; Bagnasco, G.; Costantino, U.; Marmottini, F.; Montanari, T.; Ramis, G.; Busca, G. Production of hydrogen from oxidative steam reforming of methanol: I. Preparation and characterization of Cu/ZnO/Al₂O₃ catalysts from a hydrotalcite-like LDH precursor. *J. Catal.* **2004**, *228*, 43–55. [[CrossRef](#)]
28. Pojanavaraphan, C.; Luengnaruemitchai, A.; Gulari, E. Catalytic activity of Au–Cu/CeO₂–ZrO₂ catalysts in steam reforming of methanol. *Appl. Catal. A Gen.* **2013**, *456*, 135–143. [[CrossRef](#)]
29. Yong-Feng, L.; Xin-Fa, D.; Wei-Ming, L. Effects of ZrO₂-promoter on catalytic performance of CuZnAlO catalysts for production of hydrogen by steam reforming of methanol. *Int. J. Hydrog. Energy* **2004**, *29*, 1617–1621. [[CrossRef](#)]
30. Santo, V.D.; Gallo, A.; Naldoni, A.; Guidotti, M.; Psaro, R. Bimetallic heterogeneous catalysts for hydrogen production. *Catal. Today* **2012**, *197*, 190–205. [[CrossRef](#)]
31. Rad, S.J.H.; Haghighi, M.; Eslami, A.A.; Rahmani, F.; Rahemi, N. Sol–gel vs. impregnation preparation of MgO and CeO₂ doped Ni/Al₂O₃ nanocatalysts used in dry reforming of methane: Effect of process conditions, synthesis method and support composition. *Int. J. Hydrog. Energy* **2016**, *41*, 5335–5350.
32. Li, H.; Xu, H.; Wang, J. Methane reforming with CO₂ to syngas over CeO₂-promoted Ni/Al₂O₃–ZrO₂ catalysts prepared via a direct sol-gel process. *J. Nat. Gas Chem.* **2011**, *20*, 1–8. [[CrossRef](#)]
33. Ahmed, W.; Awadallah, A.E.; Aboul-Enein, A.A. Ni/CeO₂–Al₂O₃ catalysts for methane thermo-catalytic decomposition to CO_x-free H₂ production. *Int. J. Hydrog. Energy* **2016**, *41*, 18484–18493. [[CrossRef](#)]
34. Das, D.; Llorca, J.; Dominguez, M.; Colussi, S.; Trovarelli, A.; Gayen, A. Methanol steam reforming behavior of copper impregnated over CeO₂–ZrO₂ derived from a surfactant assisted coprecipitation route. *Int. J. Hydrog. Energy* **2015**, *40*, 10463–10479. [[CrossRef](#)]
35. Mierczynski, P.; Ciesielski, R.; Kedziora, A.; Shtyka, O.; Maniecki, T.P. Methanol Synthesis Using Copper Catalysts Supported on CeO₂–Al₂O₃ Mixed Oxide. *Fibre Chem.* **2017**, *48*, 271–275. [[CrossRef](#)]
36. Li, G.; Hu, L.; Hill, J.M. Comparison of reducibility and stability of alumina-supported Ni catalysts prepared by impregnation and co-precipitation. *Appl. Catal. A Gen.* **2006**, *301*, 16–24. [[CrossRef](#)]
37. Guo, R.-T.; Zhou, Y.; Pan, W.-G.; Hong, J.-N.; Zhen, W.-L.; Jin, Q.; Ding, C.-G.; Guo, S.-Y. Effect of preparation methods on the performance of CeO₂/Al₂O₃ catalysts for selective catalytic reduction of NO with NH₃. *J. Ind. Eng. Chem.* **2013**, *19*, 2022–2025. [[CrossRef](#)]
38. Ding, M.-Y.; Tu, J.-Y.; Wang, T.-J.; Ma, L.-L.; Wang, C.-G.; Chen, L.-G. Bio-syngas methanation towards synthetic natural gas (SNG) over highly active Al₂O₃–CeO₂ supported Ni catalyst. *Fuel Process. Technol.* **2015**, *134*, 480–486. [[CrossRef](#)]
39. Kapoor, M.P.; Ichihashi, Y.; Kuraoka, K.; Shen, W.-J.; Matsumura, Y. Catalytic Methanol Decomposition over Palladium Deposited on Mesoporous Cerium Oxide. *Catal. Lett.* **2003**, *88*, 83–87. [[CrossRef](#)]
40. Kapoor, M.P.; Ichihashi, Y.; Kuraoka, K.; Matsumura, Y. Catalytic methanol decomposition over palladium deposited on thermally stable mesoporous titanium oxide. *J. Mol. Catal. A Chem.* **2003**, *198*, 303–308. [[CrossRef](#)]
41. Lenarda, M.; Moretti, E.; Storaro, L.; Patrono, P.; Pinzari, F.; Rodríguez-Castellón, E.; Jiménez-López, A.; Busca, G.; Finocchio, E.; Montanari, T.; et al. Finely dispersed Pd–Zn catalyst supported on an organized

- mesoporous alumina for hydrogen production by methanol steam reforming. *Appl. Catal. A Gen.* **2006**, *312*, 220–228. [[CrossRef](#)]
42. Chin, Y.-H.; Dagle, R.; Hu, J.; Dohnalkova, A.C.; Wang, Y. Steam reforming of methanol over highly active Pd/ZnO catalyst. *Catal. Today* **2002**, *77*, 79–88. [[CrossRef](#)]
43. Cubeiro, M.L.; Fierro, J.L.G. Selective Production of Hydrogen by Partial Oxidation of Methanol over ZnO-Supported Palladium Catalysts. *J. Catal.* **1998**, *179*, 150–162. [[CrossRef](#)]
44. Rynkowski, J.M.; Paryczak, T.; Lewicki, A.; Szyrkowska, M.I.; Maniecki, T.P.; Jóźwiak, W.K. Characterization of Ru/CeO₂-Al₂O₃ catalysts and their Performance in CO₂ Methanation. *React. Kinet. Catal. Lett.* **2000**, *71*, 55–64. [[CrossRef](#)]
45. Mierczynski, P.; Maniukiewicz, W.; Maniecki, T. Comparative studies of Pd, Ru, Ni, Cu/ZnAl₂O₄ catalysts for the water gas shift reaction (vol 11, pg 912, 2013). *Cent. Eur. J. Chem.* **2013**, *11*, 1255.
46. Zheng, W.; Zhang, J.; Ge, Q.; Xu, H.; Li, W. Effects of CeO₂ addition on Ni/Al₂O₃ catalysts for the reaction of ammonia decomposition to hydrogen. *Appl. Catal. B Environ.* **2008**, *80*, 98–105. [[CrossRef](#)]
47. Mierczynski, P.; Maniukiewicz, W.; Maniecki, T. Comparative studies of Pd, Ru, Ni, Cu/ZnAl₂O₄ catalysts for the water gas shift reaction. *Cent. Eur. J. Chem.* **2013**, *11*, 912–919.
48. Maniecki, T.; Bawolak-Olczak, K.; Mierczynski, P.; Maniukiewicz, W.; Jozwiak, W. Effect of the chemical composition of (MgO)(x)(Al₂O₃)(y) support on the catalytic performance of Ni and Ni-Au catalysts for the partial oxidation of methane. *Chem. Eng. J.* **2009**, *154*, 142–148. [[CrossRef](#)]
49. Maniecki, T.; Stadnichenko, A.; Maniukiewicz, W.; Bawolak, K.; Mierczynski, P.; Boronin, A.; Jozwiak, W. An active phase transformation on surface of Ni-Au/Al₂O₃ catalyst during partial oxidation of methane to synthesis gas. *Kinet. Catal.* **2010**, *51*, 573–578. [[CrossRef](#)]
50. Ding, M.; Tu, J.; Zhang, Q.; Wang, M.; Tsubaki, N.; Wang, T.; Ma, L. Enhancement of methanation of bio-syngas over CeO₂-modified Ni/Al₂O₃ catalysts. *Biomass Bioenergy* **2016**, *85*, 12–17. [[CrossRef](#)]
51. Wu, H.; Pantaleo, G.; la Parola, V.; Venezia, A.M.; Collard, X.; Aprile, C.; Liotta, L.F. Bi- and trimetallic Ni catalysts over Al₂O₃ and Al₂O₃-MO_x (M = Ce or Mg) oxides for methane dry reforming: Au and Pt additive effects. *Appl. Catal. B Environ.* **2014**, *156–157*, 350–361. [[CrossRef](#)]
52. Osorio-Vargas, P.; Flores-González, N.A.; Navarro, R.M.; Fierro, J.L.G.; Campos, C.H.; Reyes, P. Improved stability of Ni/Al₂O₃ catalysts by effect of promoters (La₂O₃, CeO₂) for ethanol steam-reforming reaction. *Catal. Today* **2016**, *259*, 27–38. [[CrossRef](#)]
53. Reddy, B.M.; Rao, K.N.; Reddy, G.K.; Khan, A.; Park, S.-E. Structural Characterization and Oxidehydrogenation Activity of CeO₂/Al₂O₃ and V₂O₅/CeO₂/Al₂O₃ Catalysts. *J. Phys. Chem. C* **2007**, *111*, 18751–18758. [[CrossRef](#)]
54. Jiao, Y.; Zhang, J.; Du, Y.; Li, F.; Li, C.; Lu, J.; Wang, J.; Chen, Y. Hydrogen production by catalytic steam reforming of hydrocarbon fuels over Ni/Ce-Al₂O₃ bifunctional catalysts: Effects of SrO addition. *Int. J. Hydrog. Energy* **2016**, *41*, 13436–13447. [[CrossRef](#)]
55. Luisetto, I.; Tuti, S.; Battocchio, C.; Mastro, S.L.; Sodo, A. Ni/CeO₂-Al₂O₃ catalysts for the dry reforming of methane: The effect of CeAlO₃ content and nickel crystallite size on catalytic activity and coke resistance. *Appl. Catal. A Gen.* **2015**, *500*, 12–22. [[CrossRef](#)]

